Therapeutic antibody engineering for efficient targeted degradation of membrane proteins in lysosomes

Corentin Gauthier, Morgane Daurat, Lamiaa Mohamed Ahmed Ali, Khaled El Cheikh, Iris El Bahlagui, Camille Taliercio, Elodie Morère, Magali Gary-Bobo, Alain Morère, Marcel Garcia, et al.

Biomedicine & Pharmacotherapy 175 (2024) 116707

Contents lists available at ScienceDirect

Biomedicine & Pharmacotherapy

journal homepage: www.elsevier.com/locate/biopha

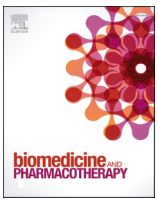

Therapeutic antibody engineering for efficient targeted degradation of membrane proteins in lysosomes

Corentin Gauthier [a,b,1], Morgane Daurat [a,1], Lamiaa Mohamed Ahmed Ali [b,c], Khaled El Cheikh [a], Iris El Bahlagui [a], Camille Taliercio [a], Elodie Morère [a,b], Magali Gary-Bobo [b], Alain Morère [b], Marcel Garcia [a], Marie Maynadier [a], Ilaria Basile [a,*]

[a] NanoMedSyn, Montpellier, France
[b] Institut des Biomolécules Max Mousseron (IBMM), University of Montpellier, CNRS, ENSCM, Montpellier, France
[c] Department of Biochemistry, Medical Research Institute, University of Alexandria, Alexandria 21561, Egypt

ARTICLE INFO

Keywords:
Targeted protein degradation
Mannose 6-phosphate receptor
Lysosome
AMFA
Mannose 6-phosphonate
Antibody engineering

ABSTRACT

Targeted degradation of pathological proteins is a promising approach to enhance the effectiveness of therapeutic monoclonal antibodies (mAbs) in cancer therapy. In this study, we demonstrate that this objective can be efficiently achieved by the grafting of mannose 6-phosphate analogues called AMFAs[2] onto the therapeutic antibodies trastuzumab and cetuximab, both directed against membrane antigens. The grafting of AMFAs confers to these antibodies the novel property of being internalized *via* the mannose 6-phosphate receptor (M6PR) pathway. AMFA conjugation to these mAbs significantly increases their cellular uptake and leads to enhanced degradation of the target antigens in cancer cells. This results in a drastic inhibition of cancer cell proliferation compared to unconjugated mAbs, as demonstrated in various cancer cell lines, and an increased therapeutic efficacy in mouse and zebrafish xenografted models. These findings highlight the potential of this technology to improve therapeutic outcomes in cancer treatment.

1. Introduction

Anti-cancer therapies are constantly evolving to become more powerful tools to fight cancer, and immunotherapy with monoclonal antibodies (mAbs) is now playing a key role in this fight. mAbs are widely used to treat cancer, recruit the immune system, or modulate the response to the treatment [1,2]. However, a growing interest in antibody research today is to make mAbs more effective and various antibody constructs and derivatives are being developed for this purpose [3]. Innovative technologies that can induce the degradation of pathogenic antigens in addition to their neutralization have emerged as a possible way to enhance the therapeutic potential of mAbs. Antigen degradation can be achieved by cellular mechanisms such as the proteasome machinery or the lysosomal catabolic function, leading to the design of complex molecules such as proteolysis-targeting chimeras (PROTACs) [4] or lysosome-targeting chimeras (LYTACs) conjugated antibodies [5]. In the search for lysosomal delivery of pathogenic proteins for their degradation, mannose 6-phosphonate derivatives (M6Pn) called AMFAs, for Analogues of Mannose 6-phosphate Functionalized at Anomeric position, represent a flexible and rapid approach to protein engineering and allow the generation of mAb-AMFA [6,7]. These functionalized analogues are highly specific for the cation-independent mannose 6-phosphate receptor (M6PR), the key receptor for lysosomal addressing of the proteins [8]. A previous study showed that the grafting of AMFAs onto therapeutic mAbs confers binding affinity for the M6PR and a high internalization rate, while preserving their affinity for the antigen and their ability to be recycled thanks to the interaction with the Fc neonatal receptor (FcRn) [9]. The AMFA technology has demonstrated its efficacy in inducing the degradation of extracellular antigens by means of AMFA-engineered antibodies [7]. We now propose to apply this technology to antibodies targeting membrane proteins involved in cancer in order to increase their efficacy by inducing the degradation of their antigen.

The study focuses on the engineering of two already marketed

* Corresponding author.
E-mail address: i.basile@nanomedsyn.com (I. Basile).
[1] These authors equally contributed to this work and share first authorship.
[2] AMFA: Analogues of the Mannose 6-phosphate Functionalized at Anomeric Position

https://doi.org/10.1016/j.biopha.2024.116707
Received 10 February 2024; Received in revised form 30 April 2024; Accepted 2 May 2024
Available online 12 May 2024

antibodies, cetuximab (CTX) and trastuzumab (TRZ), which target the epidermal growth factor receptor (EGFR)[10] and human epidermal growth factor receptor-2 (HER2) [11], respectively. These receptors, which are abnormally activated or overexpressed in various tumors, play a critical role in tumor growth by participating in the inhibition of apoptosis and increased cell proliferation. The two antibodies were grafted with AMFAs, resulting in CTX-AMFA and TRZ-AMFA, and they were chosen as models to prove the degradation of the membrane antigens, *i.e.* EGFR and HER2, respectively, by addressing them to lysosomes. We have shown that AMFA conjugation allows for greater target degradation already at low antibody concentrations and a greater anti-proliferative effect *in vitro* when cells were treated with mAb-AMFA as compared to bare mAb. Finally, *in vivo* experiments in mice or zebrafish embryos xenografted with ovarian and colorectal cancer cells demonstrated that mAb-AMFAs provided a better tumor growth inhibition than mAbs.

2. Material and methods

2.1. Cell culture

The BT-474, ZR-75-1 and LNCaP breast cancer cell lines were maintained in RPMI 1640 GlutaMax culture medium (Sigma-Aldrich, St Louis, Missouri, USA), supplemented with 10 % fetal bovine serum (FBS), 1 % penicillin-streptomycin (P/S, Sigma-Aldrich, St Louis, Missouri, USA). LNCaP medium was supplemented with 1 % sodium pyruvate, 1 % glucose and 1 % HEPES. HeLa cervical cancer, HepG2 liver cancer and A431 epidermoid carcinoma cell lines were cultured in DMEM GlutaMax culture medium (Sigma-Aldrich, St Louis, Missouri, USA) supplemented with 10 % FBS and 1 % P/S. SKOV3 ovarian cancer cell line was maintained in DMEM-F12 culture medium supplemented with 10 % FBS. HaCaT keratinocyte cell line was maintained in Keratinocytes Growth Medium 2 culture medium (Promocell, Heidelberg, Germany) supplemented with $CaCl_2$, Supplement Mix (Promocell) and with 1 % P/S. HT-29 colorectal cancer cell line was maintained in McCoy's 5 A GlutaMax culture medium (Sigma-Aldrich, St Louis, Missouri, USA) supplemented with 10 % FCS and 1 % P/S.

2.2. AMFA grafting and AMFA quantitation per antibody

The antibodies were oxidized with 1 mM sodium metaperiodate solution for CTX and 5 mM solution for TRZ at 4 °C. After 30 min, the oxidation was stopped by the addition of glycerol (20 µL/mL) and mAbs were purified on a PD-10 desalting column prepacked with G-25 Sephadex resin. AMFA was then added and kept under gentle agitation for 2 h at 37 °C. Finally, samples were dialyzed overnight against a phosphate buffer specific to the antibody. The molecular weight of the antibodies before and after AMFA grafting was determined by MALDI-TOF analysis.

2.3. mAb-AMFA characterization

Before gel loading, mAb-AMFAs and mAbs were quantified by the Bradford method and then resolved by non-reducing and reducing SDS-PAGE. After transfer to PVDF membranes, antibodies were detected with horseradish peroxidase (HRP)-conjugated secondary anti-human antibody (1:5000 dilution, Jackson ImmunoResearch) or with rabbit anti-AMFA antibody (1:1000 dilution, NanoMedSyn) and anti-rabbit HRP-conjugated antibody (1:10,000 dilution, Jackson ImmunoResearch) and incubated with ECL detection reagent (Perkin Elmer).

2.4. mAb-AMFA binding affinity for M6PR and the antigen

The affinity for the M6PR was analyzed by ELISA. 0.5 µg of M6PR were adsorbed on a Maxisorp microplate and incubated overnight at 4 °C. The plate was saturated with 2 % BSA, and then the antibodies were incubated at concentrations ranging from $5{\cdot}10^{-8}$ to $5{\cdot}10^{-6}$ M at 37 °C for 90 min. Incubation with an anti-human IgG HRP-conjugated antibody (1:5000) and the further addition of 3,3′,5,5′-tetramethylbenzidine (TMB) substrate were used to detect the antibodies bound to the coated M6PR. Absorbance was read at 650 nm.

Affinities of mAb-AMFA for their targets were quantified by ELISA. EGFR and HER2 diluted in 0.1 M carbonate buffer pH 9.6 were adsorbed on a Maxisorp microplate (Nunc) at 4 °C. Increasing antibody concentrations ranging from 0.005 to 1 pg/µL were incubated with the antigen adsorbed on the plate for 1 h at 37 °C. The mAbs retained on the plate were quantified by using anti-human IgG coupled to HRP and the addition of o-phenylenediamine dihydrochloride (OPD) substrate. Absorbances were read at 450 nm.

2.5. EGFR, HER2 and M6PR expression

A431, BT-474, HeLa, HepG2, HT-29, LNCaP, SKOV3 and ZR-75–1 cell lines were seeded in T25 flasks. Cell lysates were prepared and analyzed by Western blot to assess the EGFR, HER2 and M6PR levels. Membranes were probed with rabbit anti-EGFR antibody (1:500 dilution, ThermoFisher), mouse anti-HER2 antibody (1:500 dilution, Invitrogen), rabbit anti-M6PR antibody (1:50,000 dilution, Abcam) and anti-rabbit HRP-conjugated antibody (1:10,000 dilution, Jackson ImmunoResearch) or anti-mouse HRP-conjugated antibody (1:5000 dilution, Fisher Scientific), accordingly. GAPDH was used as a loading control by probing membranes with a mouse anti-GAPDH antibody (1:50,000 dilution, Proteintech) followed by an anti-mouse HRP-conjugated antibody (1:5000 dilution, Amersham). The proteins were detected using an ECL detection reagent (Perkin Elmer).

2.6. Assessment of mAb and mAb-AMFA internalization by confocal microscopy

HeLa, HepG2 or SKOV3 cells were treated for 5 h or 24 h with 5 nM mAb or mAb-AMFA preincubated for 15 min with 2.5 nM anti-human IgG antibody coupled with AlexaFluor647® according to manufacturer's instructions. To highlight the role of M6PR in CTX-AMFA cell uptake, an excess of 20 mM AMFA was added to the cell culture medium of HeLa cells together with CTX-AMFA to saturate M6PR and thus prevent the CTX-AMFA binding. Cell fluorescence was analyzed under confocal microscopy. Images of confocal microscopy were acquired with the ZEISS LSM880 device and analyzed with the ImageJ software.

2.7. Assessment of CTX and CTX-AMFA internalization by flow cytometry

CTX and CTX-AMFA were grafted to AlexaFluor488® dye according to manufacturer's instructions and HeLa or HepG2 cells were treated with 5 nM CTX and CTX-AMFA, respectively, for 5 h. M6PR involvement in CTX-AMFA internalization was evaluated by 20 mM AMFA addition in the culture medium. The fluorescence of the treated cells was analyzed by flow cytometry.

2.8. Degradation of HER2 protein

BT-474, ZR-75–1 and SKOV3 cells were plated at $3{\cdot}10^5$ cells/mL in 6-well plates. After 24 h, cells were treated with 5 nM TRZ or TRZ-AMFA for 5 h or 24 h. BT-474 and ZR-75–1 cell lysates were analyzed by Western blot to assess the HER2 level. Membranes were probed with a mouse anti-HER2 antibody (1:400 dilution, Invitrogen) and anti-mouse HRP-conjugated antibody (1:5000 dilution, Fisher Scientific). Actin was used as a loading control by probing membranes with a rabbit anti-actin antibody (1:1000 dilution, Abcam) and an anti-rabbit HRP-conjugated antibody (1:10,000 dilution, Jackson ImmunoResearch). The proteins were detected with ECL revelation system (Perkin Elmer) and quantified using Image J software. For the ELISA dosing, SKOV3 and ZR-75–1 cells

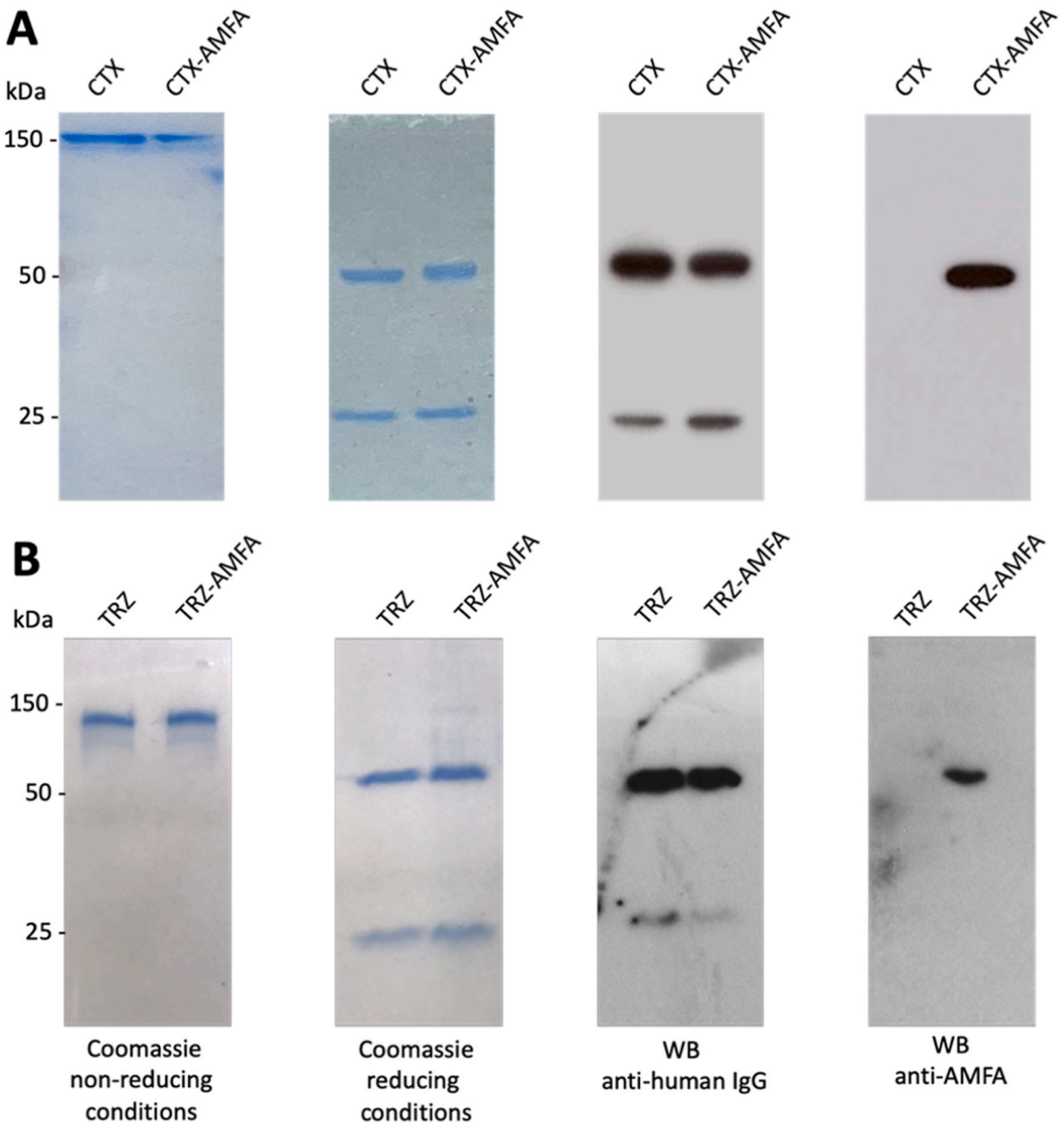

Fig. 1. Characterization of CTX and TRZ grafted with AMFA. SDS-PAGE detection of CTX (**A**) and TRZ (**B**) before and after AMFA grafting. Non-reducing and reducing SDS-PAGE analyses followed either by Coomassie blue staining of the antibodies or by Western blotting using anti-human IgG or anti-AMFA antibodies.

were lyzed and tested for HER2 level by following the manufacturer's protocol of the HER2 ELISA Kit (R&D System).

2.9. Degradation of EGFR protein

HepG2 and HT-29 cells were plated at $8{\cdot}10^5$ cells/mL in 6-well plates. After 24 h, cells were treated with 10 nM CTX or CTX-AMFA for 5 h or 24 h. Cell lysates were analyzed by Western blot to assess the EGFR level. Membranes were probed with rabbit anti-EGFR antibody (1:500 dilution, ThermoFisher) and anti-rabbit HRP-conjugated antibody (1:10,000 dilution, Jackson ImmunoResearch). Tubulin was used as a loading control by probing membranes with a mouse anti-actin antibody (1:2000 dilution, Sigma) and an anti-mouse HRP-conjugated antibody (1:5000 dilution, Fisher Scientific). The proteins were detected with ECL reagent (Perkin Elmer) and quantified using the Image J software.

2.10. Immunofluorescence detection of EGFR protein

To evaluate the localization of EGFR in cells after anti-EGFR treatment, HeLa cells were treated with 10 nM CTX or CTX-AMFA for 24 h. Then, 2 h before the end of the experiment, polyclonal anti-EGFR antibody (1:1000 dilution, Invitrogen) was added for 1 h at room temperature, then an anti-rabbit antibody coupled with FITC (1:200 dilution, Invitrogen) was incubated for 1 h at room temperature. Fluorescence was assessed by confocal microscopy with the ZEISS LSM880 device and images were analyzed with the ImageJ software to evaluate the presence of EGFR.

2.11. Anti-proliferation assay

A431 or HT-29 cells were seeded at $2{\cdot}10^4$ cells/mL in a 96-well plate and cultured for 24 h. Then, A431 and HT-29 cells were treated for 48 h with 0.5, 1, 5 and 10 nM CTX or CTX-AMFA. HeLa and ZR-75–1 cells were plated at $1{\cdot}10^4$ cells/mL and were respectively treated with 0.5, 1,

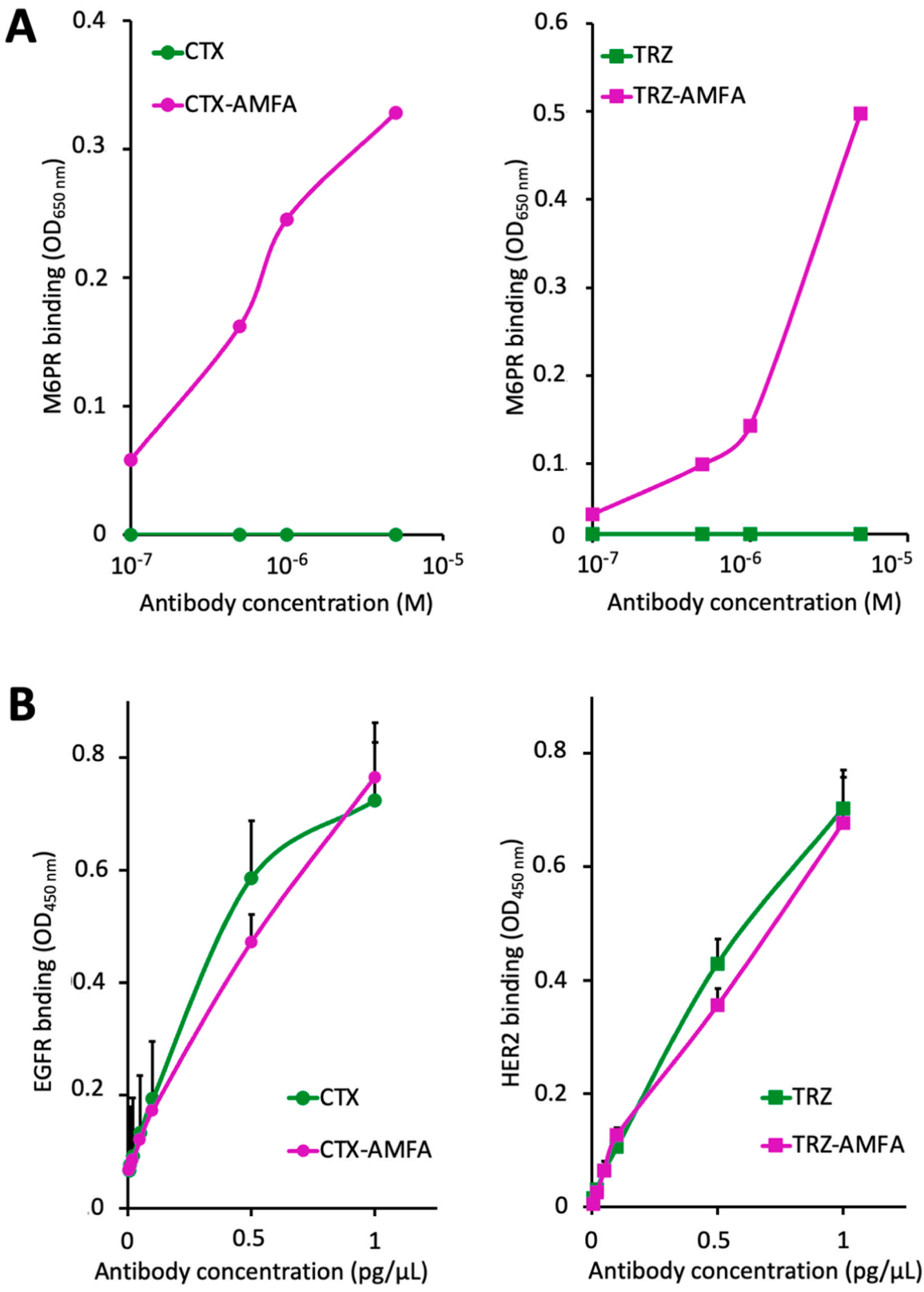

Fig. 2. Binding affinity of CTX-AMFA and TRZ-AMFA for M6PR and their target. **(A)** Binding affinity for M6PR. The affinity of CTX or CTX-AMFA (left) and TRZ or TRZ-AMFA (right) for M6PR was determined by ELISA. Results are presented as the absorbance of mAb or mAb-AMFA bound to M6PR and detected with HRP-conjugated anti-human IgG antibody. Non-specific adsorption values of the antibodies bound to uncoated wells are subtracted. **(B)** Antigen affinity. The affinity of CTX or CTX-AMFA (left) and TRZ or TRZ-AMFA (right) for EGFR and HER2, respectively, was determined by ELISA. Results are presented as the absorbance of mAb or mAb-AMFA detected by HRP-conjugated anti-human IgG antibody (mean ± SEM from triplicates).

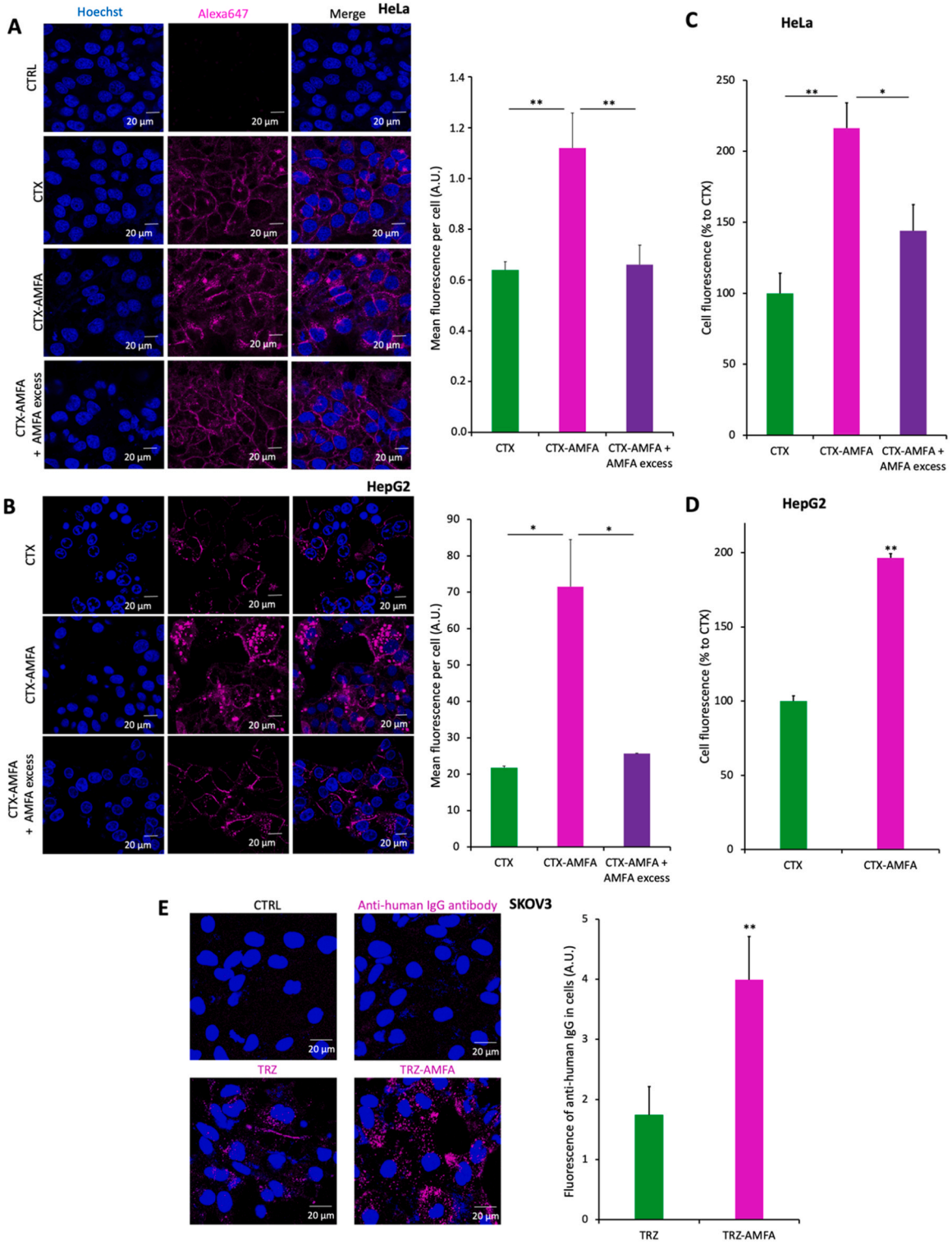

Fig. 3. Internalization of mAb and mAb-AMFA into cells. (A-B) Internalization of CTX or CTX-AMFA by confocal microscopy. HeLa cells (**A**) or HepG2 cells (**B**) were treated for 5 h with 5 nM CTX or CTX-AMFA which were detected with 2.5 nM anti-human IgG antibody coupled to AlexaFluor647®. A·20 mM AMFA excess was used to prevent the cell uptake mediated by M6PR. Results are presented as the mean fluorescence ± SEM per cell determined in 30 cells. (**C-D).** Internalization of CTX and CTX-AMFA by flow cytometry. HeLa (**C**) and HepG2 cells (**D**) were treated with 5 nM CTX or CTX-AMFA labeled with AlexaFluor488® for 5 h. An excess of 20 mM AMFA was used to inhibit CTX-AMFA cell uptake mediated by M6PR. Data are expressed as the percentage ± SEM of cell fluorescence compared to CTX (n=2). (**E**) Internalization of TRZ and TRZ-AMFA by confocal microscopy. SKOV3 cells were treated with 5 nM TRZ or TRZ-AMFA and with 2.5 nM anti-human IgG antibody coupled with AlexaFluor647® for 24 h. Microscopy was performed on living cells and data are expressed as the mean fluorescence ± SD of antibody per cell quantified in 60 cells. Tukey's test was performed for multiple comparisons. Student's t-test was performed for paired analysis: * p value < 0.05; ** p value < 0.01.

5, 10 nM CTX or CTX-AMFA and 1, 5, 20 and 50 nM TRZ or TRZ-AMFA in presence of 200 ng/mL EGF for 48 h and 72 h. After treatment, 3-[4,5-dimethylthiazol-2-yl]-2,5 diphenyl tetrazolium bromide (MTT) was added to each well and cells were incubated for 3 h at 37 °C. The absorbance was read at 540 nm.

2.12. Wound healing assay

HaCaT cells were seeded at $1{\cdot}10^6$ cells/mL in 6-well plates and cultured for 24 h. Then, a scratch was realized on confluent cells with a 200 µL tip to mimic a wound. The scratched area was photographed. Cells were treated with 10 nM CTX or CTX-AMFA for 72 h. Imaging was performed at 24, 48 and 72 h to monitor the scratched area. The wound area was then analyzed by ImageJ and the results were calculated as the area relative to the area at 0 h of treatment.

2.13. Treatment of mice xenografted with SKOV3 cells

Animal experiments were performed in accordance with the European guidelines (Directive 2010/63/EU) and approved by the Languedoc-Roussillon Animal Research Ethics Committee (CEEA-LR n°36) and the French Ministry of Higher Education and Research (#35530-20220221154253). To assess the efficacy of TRZ-AMFA *in vivo*, 5–6 week old Balb/c nude mice were injected subcutaneously with SKOV3 cells at $2{\cdot}10^6$ cells/100 µL in the right flank. When xenografted tumors reached 50 mm^3 according to the formula $(w^2 \times l) \times 0.52$, where w is the width and l is the length, mice were randomly divided into three homogeneous groups and received 8 weekly intraperitoneal injections of vehicle alone, i.e. a saline solution (CTRL group), 6 mg/kg TRZ (TRZ group) or 6 mg/kg TRZ-AMFA (TRZ-AMFA group). Mice were constantly monitored for their health status and weighed weekly, and tumors were measured with a caliper. At the end of the experiment, animals were euthanized, and tumors and tissues were collected.

2.14. Treatment of zebrafish embryos xenografted with HT-29 or SKOV3 cells

The *casper* zebrafish strain was purchased from the Zebrafish International Resource Center (EIRC). The animals were housed and cared at the zebrafish platform of Molecular Mechanisms in Neurodegenerative Dementia (MMDN) Unit, Inserm U1198, University of Montpellier according to European guidelines.

Experiments were conducted on zebrafish embryos in accordance with the EU Directive 2010/63/EU on the protection of animals used for scientific purposes and approved by the Languedoc-Roussillon Animal Research Ethics Committee (CEEA-LR n°.36) and the French Ministry of Higher Education and Research (#8884–2017021011315319).

48 h after seeding, HT-29 or SKOV3 cells were treated for 24 h with 10 nM CTX or CTX-AMFA, or 5 nM TRZ or TRZ-AMFA, respectively. After incubation, the cells were washed twice with PBS, trypsinized and then incubated with 2 µg/mL of Dil Stain (1,1'-dioctadecyl-3,3,3',3'-tetramethylindocarbocyanine perchlorate, Invitrogen) for 15 min at 37 °C. Embryos were anesthetized with 168 mg/L tricain, placed in the agarose mold and injected by receiving 1–3 pulses of 3 nL of cell suspension ($3{\cdot}10^7$ cells/mL) into the pericardial cavity then kept in water at 31 °C. After 24 h, embryos were injected intravenously with 5 % glucose solution (CTRL) or with 5 ng *per* embryo of CTX or CTX-AMFA diluted in 5 % glucose solution or with 3.6 ng *per* embryo of TRZ or TRZ-AMFA diluted in 5 % glucose solution. After injection embryos were imaged using EVOS5000 microscope (T0). Embryos were then allowed to develop at 31 °C and were observed at 24, 48 and 72 h post injection (hpi). The fluorescence relative to the area of the cancer cell xenografts was quantified using ImageJ software.

2.15. Statistical analysis

Statistical analyses were performed by using GraphPad prism 8.0. Student's t-test and Tukey's test were used to determine statistical differences between the means of *in vitro* experiments. Tukey's test was used to perform one-way ANOVA and mixed effect analysis for multiple comparisons in *in vivo* experiments. Fisher's exact test was performed to assess the significance of the difference between the number of individuals with metastases. A p-value of less than 0.05 ($p < 0.05$), 0.01 ($p < 0.01$), 0.001 ($p < 0.001$) or 0.0001 ($p < 0.0001$) was considered statistically significant.

3. Results

3.1. Characterization of AMFA grafting onto mAb

The AMFA was grafted onto the oligosaccharide chains of CTX and TRZ as previously described [9], and mAb and mAb-AMFA were first analyzed by SDS-PAGE. As shown in Fig. 1 with Coomassie staining under non-reducing conditions, only the characteristic protein band at 150 kDa is present, indicating no visible antibody degradation related to the grafting process. This observation was confirmed by Coomassie staining under reducing conditions as well as by Western blot with anti-human IgG detection, where both heavy chains (55 kDa) and light chains (25 kDa) were observed. Finally, AMFA were detected only on the heavy chains of CTX-AMFA (Fig. 1**A**) and TRZ-AMFA (Fig. 1**B**), with no signal on the light chains. The grafting was confirmed by MALDI-TOF analysis which showed the grafting of 3.8 ± 0.2 AMFA for TRZ-AMFA (n=5) and 3.8 ± 0.5 for CTX-AMFA (n=3).

3.2. Affinity of mAb-AMFA for M6PR and their antigens

To analyze the effects of the AMFA grafting to mAbs, the gain of affinity for M6PR and the affinity for their respective antigens were examined. Fig. 2**A** clearly shows that AMFA grafting enables CTX and TRZ to acquire a high affinity for M6PR, compared to an undetectable affinity for unconjugated mAbs. In Fig. 2**B**, CTX-AMFA and TRZ-AMFA have the same affinity for their antigens, EGFR and HER2, respectively, as their unmodified counterparts. These results indicate that AMFA grafting confers to the antibodies the ability to bind the M6PR with a high affinity without affecting the affinity for their targets.

3.3. Cellular levels of EGFR, HER2 and M6PR

The levels of M6PR, HER2 and EGFR were evaluated in the different cell lines used for the experiments. All cells do express the M6PR, although at different levels (Fig. S1). The prostate cancer cell line LNCaP was used as a control for M6PR overexpression [12]. Concerning EGFR expression, the cells used for CTX experiments all express EGFR, and in particular the A431 cells overexpress it. For HER2 expression, the BT-474 cell line overexpresses the receptor, while the other two cell lines, SKOV3 and ZR-75–1, show the same level of expression. These results are important to evaluate the efficacy of mAb-AMFA treatment as a function of the receptor level.

3.4. Internalization of mAb-AMFA into cells

The internalization of mAb and mAb-AMFA was first assessed by confocal microscopy. An increase in the fluorescence was observed in the presence of CTX-AMFA in HeLa and HepG2 cells after 5 h of treatment, 1.75-fold and 3.4-fold higher than CTX, respectively (Fig. 3**A-B**). Interestingly, in both cell lines, the increased fluorescence was reversed by the addition of AMFA excess, which saturates the M6PR and thus prevents CTX-AMFA binding. Indeed, the level of CTX-AMFA fluorescence decreased close to the CTX level, highlighting the key role of M6PR in CTX-AMFA cell internalization (Fig. 3**A**). In addition, the

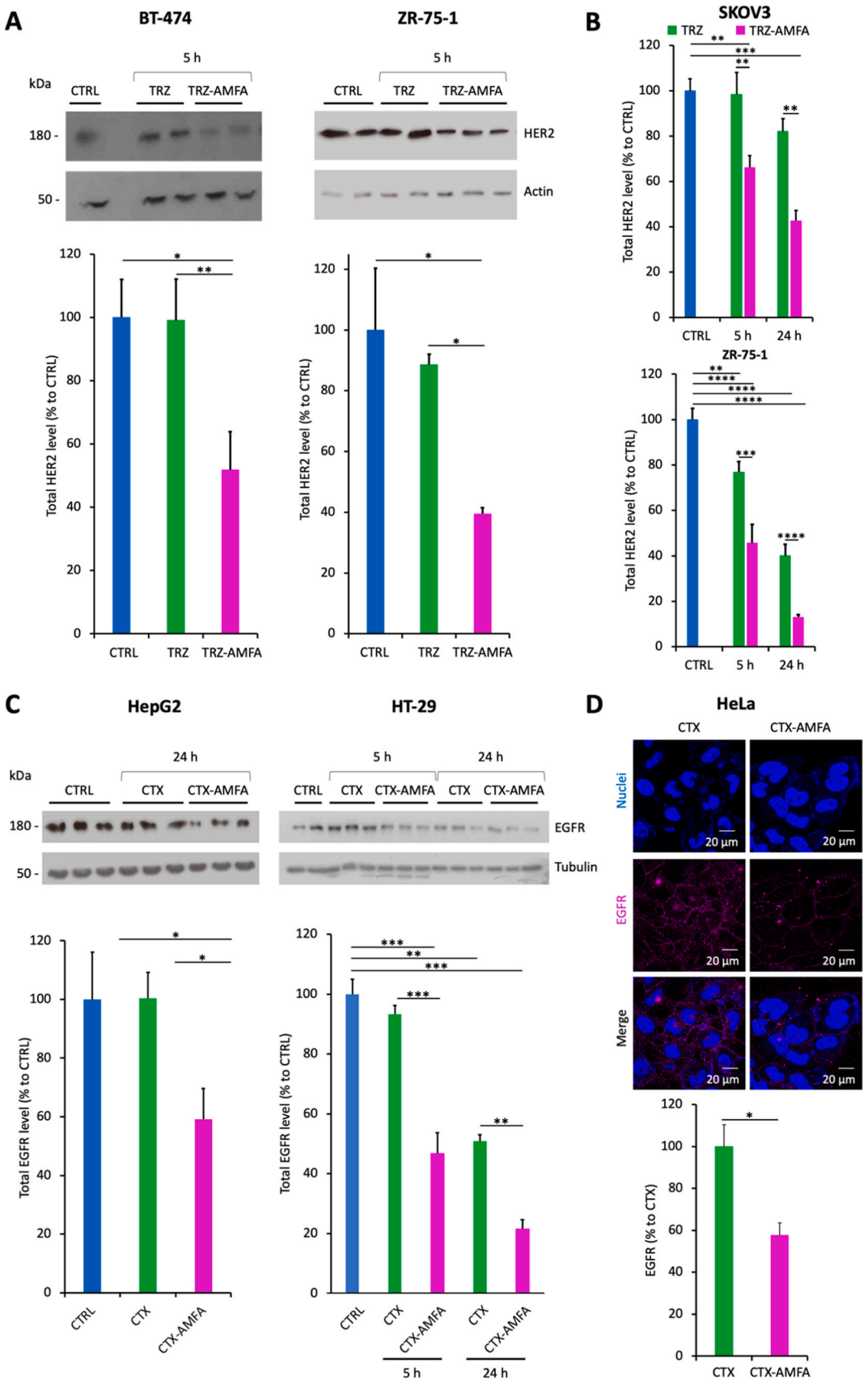

(caption on next page)

Fig. 4. Degradation of HER2 and EGFR proteins. (A) HER2 degradation analysis in BT-474 and ZR-75–1 cells at 5 h by Western blot. Cells were treated with 5 nM TRZ or TRZ-AMFA for 5 h (n=2) and analyzed by Western blot. **(B)** HER2 degradation at 5 h and 24 h in SKOV3 and ZR-75–1 cells. Cells were treated with 5 nM TRZ or TRZ-AMFA for 5 h or 24 h and HER2 levels were determined by ELISA (n=2). **(C)** EGFR degradation in HepG2 (left) or HT-29 cells (right). Cells were treated with 10 nM CTX or CTX-AMFA for 5 h or 24 h. One representative experiment out of two is shown. For Fig. A-C, membrane receptor levels were quantified and expressed as the percentage ± SEM of total HER2 or EGFR levels in control cells, accordingly. **(D)** EGFR membrane detection by confocal microscopy. HeLa cells were treated with 10 nM CTX or CTX-AMFA for 24 h and EGFR was detected with an anti-EGFR antibody together with a secondary antibody coupled with AlexaFluor647®. Microscopy was performed on living cells and EGFR quantification is presented as the mean fluorescence ± SEM of antibody per cell determined in 40 cells. Statistical analysis was performed with Tukey's multiple comparison test and Student's t-test:* p value < 0.05; ** p value < 0.01; *** p value < 0.001; **** p value < 0.0001.

internalization was also evaluated by flow cytometry experiments using the same cell lines. As shown in Fig. 3**C-D** CTX-AMFA fluorescence is increased by 2.2-fold and 1.9-fold in HeLa and HepG2 cells, respectively, compared to that of CTX, and, when an excess of AMFA was added, the fluorescence decreased to the level of CTX. Similarly, a 2.3-fold higher fluorescence of TRZ-AMFA as compared to TRZ was observed after 24 h of treatment in SKOV3 cells (Fig. 3**E**). These results demonstrate that AMFA grafting significantly increases mAb uptake through an M6PR-mediated mechanism.

3.5. HER2 and EGFR degradation

The degradation of HER2 and EGFR proteins was investigated to demonstrate the improved efficacy of the AMFA engineered mAb. HER2 protein levels were first analyzed by Western blot in BT-474 and ZR-75–1 cells treated with 5 nM TRZ or TRZ-AMFA. As shown in Fig. 4**A**, the cellular level of HER2 decreased by 49 % and 61 % in BT-474 (left) and ZR-75–1 (right) cell lines, respectively, after TRZ-AMFA treatment, whereas the HER2 level did not significantly decrease with TRZ treatment in either cell line after 5 h. HER2 protein levels were also analyzed by ELISA in SKOV3 and ZR-75–1. In SKOV3 cells, TRZ-AMFA treatment was significantly more effective than TRZ in reducing HER2 levels at 5 h and 24 h. In ZR-75–1 cells, the degradation of HER2 by TRZ is higher at 24 h compared to SKOV3 cells. However, the HER2 levels were more significantly decreased by TRZ-AMFA (up to 87 % after 24 h), demonstrating the higher efficacy of TRZ-AMFA (Fig. 4**B**). EGFR degradation was assessed in HepG2 and HT-29 cells after treatment with 10 nM CTX and CTX-AMFA (Fig. 4**C**). The total EGFR level in HepG2 cells treated with CTX-AMFA decreased by 40 % after 24 h, while no change in EGFR level was observed with CTX treatment. In HT-29 cells, EGFR protein level decreased by 53 % in CTX-AMFA treated cells compared to untreated cells, while CTX reduced EGFR level by only 7 % after 5 h of treatment. After 24 h of treatment, only 22 % of EGFR was present in CTX-AMFA-treated cells and more than 50 % was present in CTX-treated cells. To complement these data, the location of EGFR at the membrane of HeLa cells was analyzed by confocal microscopy. EGFR was observed at the membrane of CTX treated cells, while the signal corresponding to EGFR decreased by 42 % in the cells treated with CTX-AMFA. This result was confirmed by signal quantification, which showed a significant decrease in the presence of EGFR at the cell membrane (Fig. 4**D**). Taken together, these results provide evidence for the enhanced *in vitro* efficacy of mAb-AMFA in degrading EGFR and HER2 proteins.

3.6. Antiproliferative effect of mAb-AMFA

The antiproliferative effect of CTX-AMFA was first evaluated in A431 and HT-29 cells at concentrations ranging from 0.5 to 10 nM for 48 h. In both cell lines, CTX-AMFA treatment induced a 2-fold greater antiproliferative effect than CTX at the different concentrations (Fig. 5**A-B**). Another way to demonstrate the antiproliferative effect of TRZ-AMFA and CTX-AMFA was to reverse the mitogenic effect induced by the addition of EGF. Fig. 5**C** shows that CTX-AMFA has a better ability to reverse the proliferative effect of EGF than CTX, even at low antibody concentrations. The same response was observed with TRZ-AMFA in ZR-75–1 cells (Fig. 5**D**). These results suggest that AMFA-grafting enhances the antiproliferative effect of CTX and TRZ *in vitro*.

3.7. Effects of mAb-AMFA on wound healing assay

To further emphasize the improved *in vitro* efficacy of mAb-AMFA, a wound healing assay was performed using a validated cell model, HaCaT cells. Cells were treated with 10 nM CTX or CTX-AMFA for up to 72 h and the remaining free area was compared to that at time 0. Fig. 6**A** shows images of the scratched area over time. It can be seen that under control conditions, the free area is rapidly covered by cells, whereas CTX-treated cells cover the scratched area more slowly. In addition, CTX-AMFA appears to be more effective than CTX in slowing down the coverage of the free area. These observations were confirmed by the quantification of the remaining free area (Fig. 6**B**). Indeed, a better efficacy for CTX-AMFA was observed throughout the treatment period. Interestingly, at 48 h post-treatment, CTX-AMFA prevented the normal recovery by 31 % versus 22 % with the CTX treatment (Fig. 6**B**). These findings suggest a greater ability of mAb-AMFA to prevent wound healing through a mechanism involving cell proliferation and migration.

3.8. In vivo efficacy for reducing tumor growth in zebrafish embryos and mice

The efficacy of mAb and mAb-AMFA was first investigated *in vivo* using zebrafish embryos as an integrated model of human tumor growth. At 72 hpi, tumor growth was significantly reduced in CTX-AMFA treated embryos compared to CTRL and CTX treated animals, by 33.3 % and 27.3 %, respectively (Fig. 7**A**). Moreover, CTX-AMFA significantly reduced metastasis formation, since more than 66 % of CTRL individuals presented metastases, compared to 21.4 % of CTX-treated individuals and only 6.3 % of CTX-AMFA treated individuals. (Fig. 7**B**). In the zebrafish model xenografted with SKOV3 cells, TRZ-AMFA reduced tumor growth by 48.1 % as compared to CTRL while TRZ reduced tumor growth by only 20 % at 72 hpi (Fig. 7**C**).

The effect of AMFA grafting in improving the therapeutic efficacy was then evaluated in the BALB/c nude$^{nu/nu}$ mouse model xenografted with human SKOV3 cells. Xenografted mice received 8 weekly injections of either 6 mg/kg TRZ or TRZ-AMFA and the tumor area was measured once a week. Although TRZ was already effective in reducing the tumor size at this dose, AMFA grafting managed to enhance the anti-tumor response to the therapeutic antibody (Fig. 7**D**). This difference was significant when comparing two tumor growth curves. These data indicate a greater anti-tumor efficacy of mAb-AMFA compared to mAb.

4. Discussion

Conventional immunotherapies based on monoclonal antibodies typically tend to regulate or modulate a biological activity. They are often proposed as a second or third line of treatment and in most cases as an adjunct to invasive therapies such as chemotherapy or radiotherapy.

In order to obtain more efficient mAbs, there has been an increasing interest in targeted degradation of the antigen. This approach requires both the ability to target the component of interest and the ability to transport and internalize the resulting complex into cells for degradation.

The key receptor for targeting proteins to lysosomes, the organelles responsible for the degradation of intracellular and extracellular material, is the M6PR. This receptor has been shown to be an effective

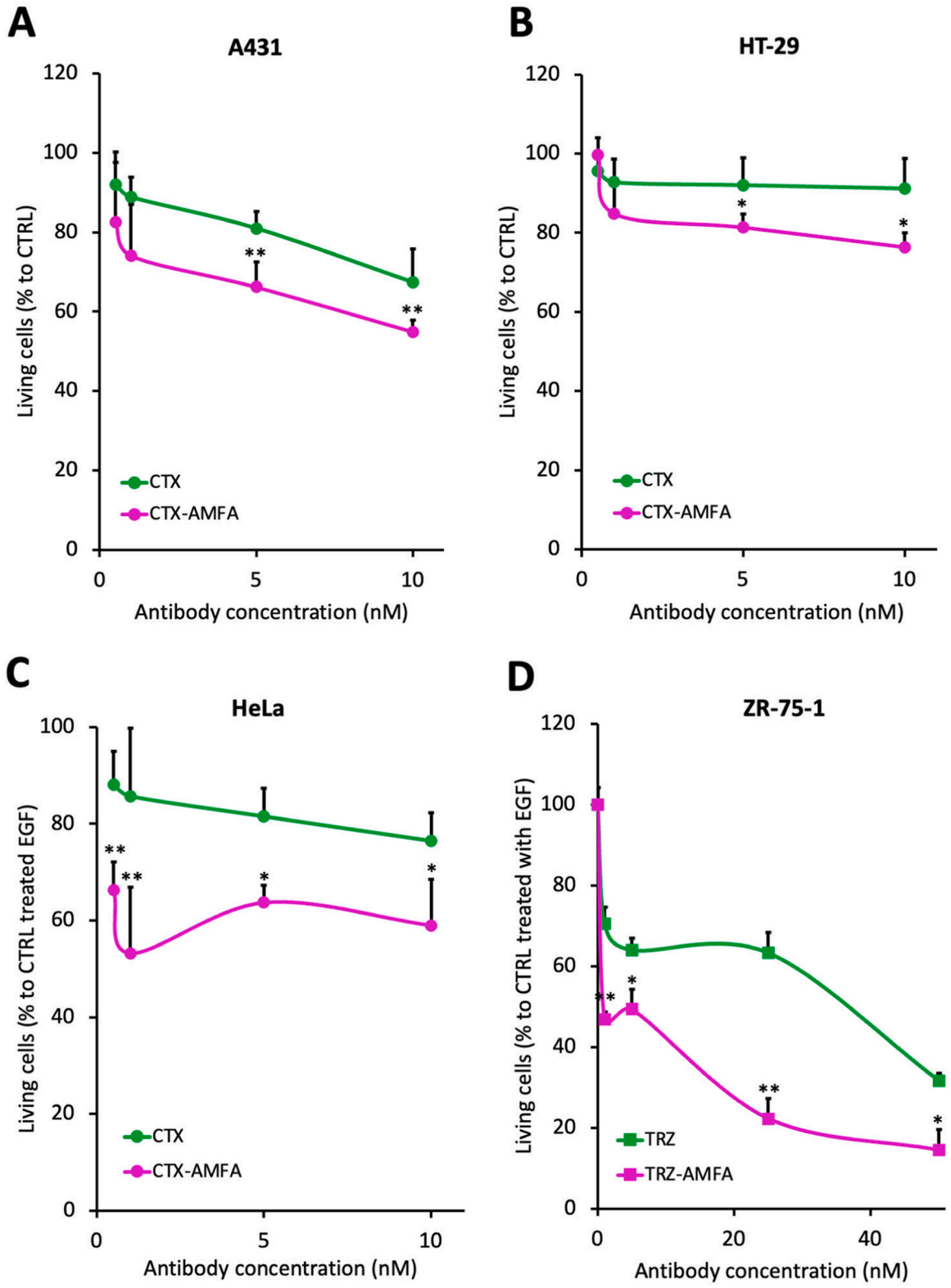

Fig. 5. Antiproliferative effect of mAb and mAb-AMFA. Antiproliferative effect of CTX and CTX-AMFA in A431 (**A**) and HT-29 (**B**) cells. A431 and HT-29 cells were treated with 0.5–10 nM CTX or CTX-AMFA for 48 h and cell proliferation was analyzed by MTT assay. Results are presented as the percentage ± SD of living cells compared to control (n=2). **(C)** Antiproliferative effect of CTX and CTX-AMFA in the presence of EGF. HeLa cells were treated with 0.5–10 nM CTX or CTX-AMFA in the presence of 200 ng/mL EGF for 48 h (n=3). **(D)** Antiproliferative effect of TRZ or TRZ-AMFA in the presence of EGF. ZR-75–1 cells were treated with 1–50 nM TRZ or TRZ-AMFA in the presence of 200 ng/mL EGF for 72 h (n=2). Cell proliferation was analyzed by MTT assay. Data are expressed as the percentage ± SD of living cells relatively to control cells treated with EGF. Student's t-test: * p value < 0.05; ** p value < 0.01.

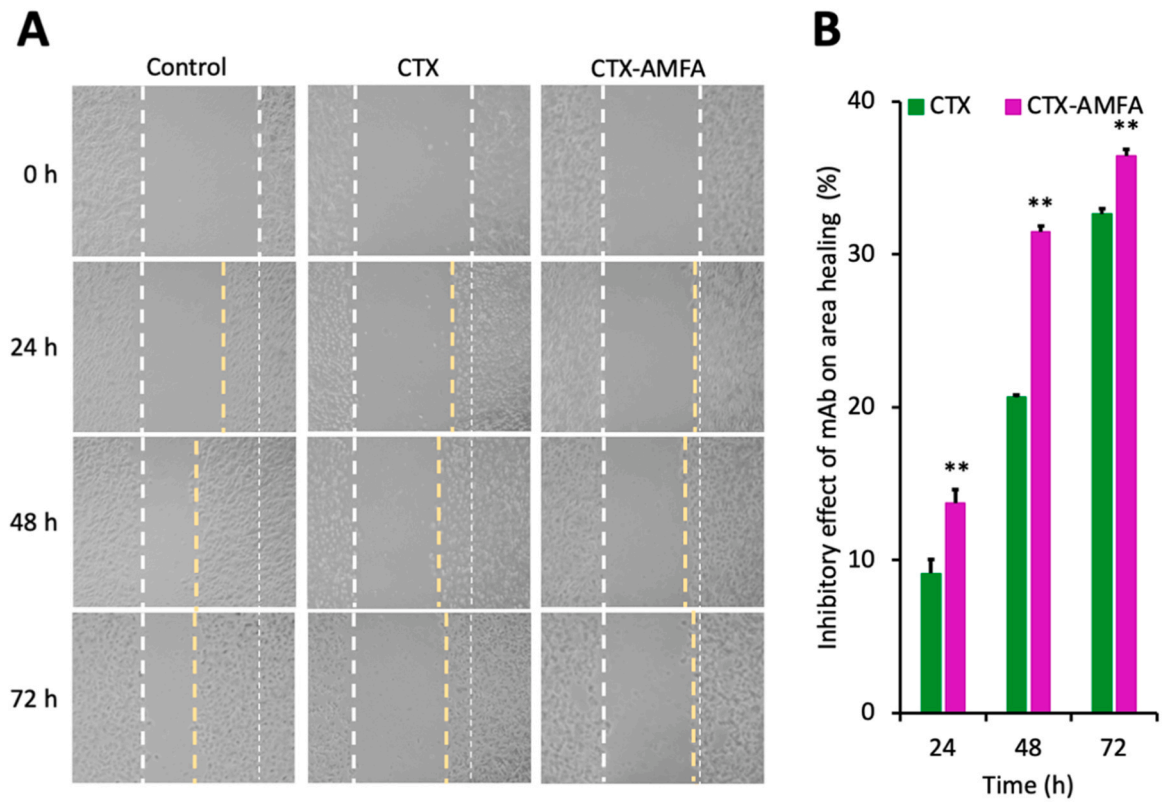

Fig. 6. Increased anti-migration and anti-proliferative effects of CTX-AMFA. HaCaT cells were treated with 10 nM CTX or CTX-AMFA for 72 h. A wound healing test was realized and the scratch area was monitored at 24, 48 and 72 h to assess the cell migration and proliferation. **(A)** Wound healing test at 0 h, 24 h, 48 h and 72 h after treatment. **(B)** Increment in the free area by CTX and CTX-AMFA. Free areas were quantified at different time points and compared to the area at time 0 h. Results are presented as the percentage of the free area variation in mAb treated cells over time compared to the free area variation in untreated control cells. Mean ± SD. Student's t-test: ** p value < 0.01.

transporter for the delivery of proteins or macromolecules to lysosomes and the AMFAs have been shown to be a powerful tool for targeting the M6PR [6,9,12–17]. Once grafted to the molecule of interest, these derivatives allow drugs or proteins to be addressed to lysosomes. This property maximizes the number of molecules that can bind the M6PR and reach the lysosome. Proper degradation of the particular compound of interest in the pathological tissue requires a highly regulated targeting. This selectivity for the target can be achieved by the use of antibodies. Banik et *al.* demonstrated the *in vitro* degradation of membrane proteins using LYTACs, which consist of mAbs directed against different membrane receptors grafted with large polyglycopeptides containing numerous analogues of M6P, which were developed on the basis of AMFA [5]. The LYTAC technology takes advantage of the lysosomal machinery to degrade extracellular proteins and the initial results are encouraging. However, due to the size of the glycopeptides, which contain 20–90 M6Pn units, a potential immunogenic issue can be foreseen, as a strong immunogenic response is observed in the presence of a high number of glycans [18]. The AMFA technology allows for controlled glycosylation with a reduced number of analogues, which may limit the immunogenic side effects. In addition, previous *in vivo* experiments have shown that AMFA grafting to proteins is safe and does not induce an immunogenic response, even after several months of treatment [6]. In addition, AMFA engineering on mAbs directed against soluble antigens has effectively induced the degradation of extracellular antigens in the lysosomes, thereby significantly reducing their biological effects [7].

Here, we have demonstrated the potential of AMFA to promote the degradation of membrane proteins *via* the M6PR pathway. As a proof of concept, we chose to target two membrane receptors involved in tumor growth, EGFR and HER2 and we selected two commercially available mAbs directed against these receptors. In this study, we have shown a reproducible and validated method for grafting AMFA onto antibodies. Indeed, this grafting allows antibodies to acquire a high affinity for M6PR without reducing their affinity for their target, here the HER2 and EGFR proteins. Moreover, analogously to previous published data on different mAbs, the ability of these two mAb-AMFAs to be recycled and released into the extracellular compartment is unaltered (data not shown). We have proved that regardless of the cell line used, AMFA grafting significantly increases the mAb uptake compared to unconjugated mAb, and this improvement is mediated by M6PR. Interestingly, studies carried out in different cell lines have shown that M6PR expression is ubiquitous but variable. In addition, we have demonstrated that mAb-AMFA enables greater internalization and degradation of membrane targets in cells expressing both high and low levels of pathogenic proteins. Since the EGFR and HER2 proteins are involved in cell proliferation, degradation of these receptors is expected to reduce cell proliferation. Indeed, mAb-AMFA was able to inhibit cell proliferation to a greater extent than mAb, even at low antibody concentrations. Finally, we have demonstrated superior *in vivo* efficacy of CTX-AMFA and TRZ-AMFA compared to unmodified antibodies in inhibiting tumor growth in two integrated models, zebrafish embryos and mice.

Taken together, these data indicate that the grafting of AMFA to mAb is an effective way to induce the degradation of extracellular pathogenic molecules in lysosomes. As shown in this study, the enhanced efficacy observed in different cell lines, regardless of M6PR expression levels, makes it possible to envisage an application to a wide range of pathologies, as well as an adaptation to antibodies already effective in the clinic, such as trastuzumab. In addition to the lysosomal targeting, the higher efficacy in degrading membrane antigens may be due to the repeated cycles that mAb-AMFA undergoes: the M6PR-mediated cellular

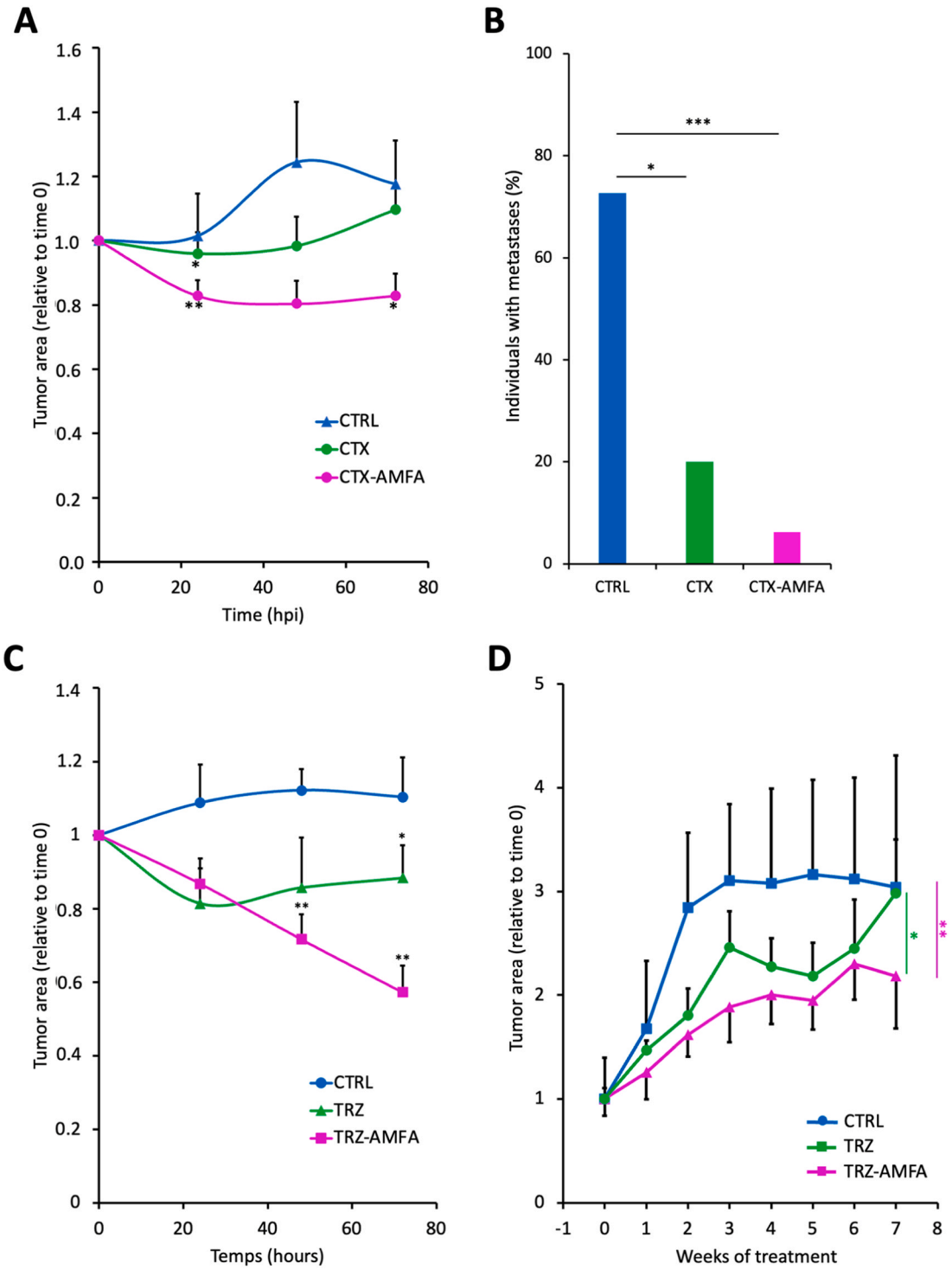

Fig. 7. Growth inhibition of xenografted tumors by mAb and mAb-AMFA in zebrafish embryos and mice. (A) Tumor growth inhibition in casper zebrafish xenografted embryos treated with CTX or CTX-AMFA. Embryos were xenografted with human HT-29 cells and intravenously injected with 5 ng of CTX (n=15) or CTX-AMFA (n=16) or 5 % glucose solution for CTRL group (n=11) and were monitored for 72 hpi. Data represent tumor growth rate ± SEM over time. One-way ANOVA Tukey's test was realized for statistical analysis. At 24 h, CTRL/CTX-AMFA p value < 0.01, CTRL/CTX p value < 0.05; at 72 h CTRL/CTX-AMFA p value < 0.05 (**B**) Metastasis development. Data represent the percentage of untreated or CTX or CTX-AMFA treated embroys presenting at least one metastasis at 72 hpi. Fisher's exact test was performed for statistical analysis. (**C**) Tumor growth inhibition in casper zebrafish xenografted embryos treated with TRZ or TRZ-AMFA. Embryos were xenografted with human SKOV3 cells and intravenously injected with 3.6 ng TRZ (n=9) or TRZ-AMFA (n=9) or 5 % glucose solution for control (CTRL, n=7) and were monitored for 72 hpi. Data represent the tumor growth rate ± SEM over time. One-way ANOVA Tukey's test was realized for statistical analysis. At 48 h CTRL/TRZ-AMFA p value < 0.01, at 72 h CTRL/TRZ-AMFA p value < 0.01 and TRZ/TRZ-AMFA p value < 0.05 (**D**). Tumor growth inhibition in xenografted mice treated with TRZ and TRZ-AMFA. BALB/c nude$^{nu/nu}$ female mice were xenografted with human SKOV3 cells and received 8 weekly injections of 6 mg/kg TRZ (n=6) or TRZ-AMFA (n=6) or PBS for control mice (CTRL; n=4). Data represent the mean ± SEM of tumor area relative to time 0 over treatment weeks. Mixed effect analysis model together with Tukey's test was performed for statistical analysis to compare treatment curves. CTRL/TRZ-AMFA p <0.01, TRZ/TRZ-AMFA p <0.05. * p value < 0.05; ** p value < 0.01; *** p value < 0.001.

uptake of mAb-AMFA-antigen followed by FcRn-mediated recycling of the mAb-AMFA back to the cell membrane where it can bind the antigen again. In a recent study, this recycling of mAb-AMFA was demonstrated with other antigens, and AMFA binding to mAb was shown to be stable for 21 days in mice [9]. The development of drugs for targeting pathological extracellular proteins is regularly confronted with the difficulty of completely inhibiting their functions. By degrading the membrane antigen, a pathology currently known as "undruggable" could be transformed into "druggable" [19–21]. These promising results using therapeutic antibodies support the development of AMFA-engineered antibodies for membrane antigen degradation.

5. Conclusion

This work has demonstrated that the AMFA technology is able to efficiently internalize immune complexes into cells for antigen degradation and increase the therapeutic efficacy of the antibody. These findings open up a new avenue for targeting pathogenic proteins, that could lead to new therapeutics.

Ethics approval

Animal experiments were approved by the Languedoc-Roussillon Animal Research Ethics Committee (CEEA-LR n°.36) and the French Ministry of Higher Education and Research #35530-20220221154253 for mice and #8884-2017021011315319 for zebrafish studies, respectively, and performed in accordance with the European Union guidelines regulated under Directive 2010/63/EU on the protection of animals used for scientific purposes.

Funding

This work was supported by the Contrat Innovation grant from the Région Occitanie (France). CG and EM received a CIFRE grant from the National Association of Research and Technology (ANRT) to partially finance their PhD scholarship.

CRediT authorship contribution statement

Corentin Gauthier: Conceptualization, Formal analysis, Investigation, Visualization, Writing-original draft, Writing-review & editing. **Morgane Daurat:** Conceptualization, Formal analysis, Investigation, Visualization, Writing-original draft, Writing-review & editing. **Lamiaa Mohamed Ahmed Ali:** Investigation, Validation, Writing-original draft. **Khaled El Cheikh:** Investigation, Formal analysis, Validation, Writing-original draft. **Iris El Bahlagui:** Investigation, **Camille Taliercio:** Investigation, **Elodie Morère:** Investigation, Resources, **Magali Gary-Bobo:** Supervision, Writing-original draft. **Alain Morère:** Supervision, Validation, Writing-original draft. **Marcel Garcia:** Conceptualization, Supervision, Validation, Writing-original draft, Writing-review & editing. **Marie Maynadier:** Conceptualization, Investigation, Supervision, Project Administration, Writing-original draft, Writing-review & editing. **Ilaria Basile:** Conceptualization, Project Administration, Investigation, Supervision, Validation, Writing-original draft, Writing-review & editing.

Declaration of Competing Interest

The authors declare that they have no known competing financial interests or personal relationships that could have appeared to influence the work reported in this paper

Data availability

Data will be made available on request.

Acknowledgments

We are grateful to the RAM-CECEMA facilty of the University of Montpellier for animal housing and their support for the *in vivo* experiments in mice. We also thank the zebrafish platform of Molecular Mechanisms in Neurodegenerative Dementia (MMDN) Unit, Inserm U1198, University of Montpellier for animal housing. We acknowledge the Montpellier imaging platform MRI, member of the France-BioImaging national infrastructure which is supported by the French National Research Agency (ANR-10-INBS-04, Investments for the Future), for providing equipment and assistance with the confocal microscopy experiments. We thank ANRT for CG (N° 2020/1208) and EM (N°2021/1028) fellowships and Region Occitanie for Innovation Grant N° 20017014.

Appendix A. Supporting information

Supplementary data associated with this article can be found in the online version at doi:10.1016/j.biopha.2024.116707.

References

[1] G.P. Adams, L.M. Weiner, Monoclonal antibody therapy of cancer, Nat. Biotechnol. 23 (2005) 1147–1157, https://doi.org/10.1038/nbt1137.
[2] M. Kumar, A. Jalota, S.K. Sahu, S. Haque, Therapeutic antibodies for the prevention and treatment of cancer, J. Biomed. Sci. 31 (2024) 6, https://doi.org/10.1186/s12929-024-00996-w.
[3] S. Jin, Y. Sun, X. Liang, X. Gu, J. Ning, Y. Xu, et al., Emerging new therapeutic antibody derivatives for cancer treatment, Signal Transduct. Target. Ther. 7 (2022) 39, https://doi.org/10.1038/s41392-021-00868-x.
[4] K.M. Sakamoto, K.B. Kim, A. Kumagai, F. Mercurio, C.M. Crews, R.J. Deshaies, Protacs: chimeric molecules that target proteins to the Skp1-Cullin-F box complex for ubiquitination and degradation, Proc. Natl. Acad. Sci. U. S. A. 98 (2001) 8554–8559, https://doi.org/10.1073/pnas.141230798.
[5] S.M. Banik, K. Pedram, S. Wisnovsky, G. Ahn, N.M. Riley, C.R. Bertozzi, Lysosome-targeting chimaeras for degradation of extracellular proteins, Nature 584 (2020) 291–297, https://doi.org/10.1038/s41586-020-2545-9.
[6] K. El Cheikh, I. Basile, A. Da Silva, C. Bernon, P. Cérutti, F. Salgues, et al., Design of potent mannose 6-phosphate analogues for the functionalization of lysosomal enzymes to improve the treatment of pompe disease, Angew. Chem. Int. Ed. Engl. 55 (2016) 14774–14777, https://doi.org/10.1002/anie.201607824.
[7] M. Daurat, C. Gauthier, K. El Cheikh, L.M.A. Ali, E. Morère, N. Bettache, et al., Engineered therapeutic antibodies with mannose 6-phosphate analogues as a tool to degrade extracellular proteins, Front. Immunol. 15 (2024) 1273280, https://doi.org/10.3389/fimmu.2024.1273280.
[8] C. Gauthier, K. El Cheikh, I. Basile, M. Daurat, E. Morère, M. Garcia, et al., Cation-independent mannose 6-phosphate receptor: From roles and functions to targeted therapies, J. Control. Release 365 (2024) 759–772, https://doi.org/10.1016/j.jconrel.2023.12.014.
[9] C. Gauthier, J. Mariot, M. Daurat, C. Dhommée, K. El Cheikh, E. Morère, et al., Mannose 6-phosphate receptor-targeting antibodies preserve Fc receptor-mediated recycling, J. Control. Release 358 (2023) 465–475, https://doi.org/10.1016/j.jconrel.2023.05.011.
[10] B. Vincenzi, A. Zoccoli, F. Pantano, O. Venditti, S. Galluzzo, CETUXIMAB: from bench to bedside, Curr. Cancer Drug Targets 10 (2010) 80–95, https://doi.org/10.2174/156800910790980241.
[11] H. Maadi, M.H. Soheilifar, W.-S. Choi, A. Moshtaghian, Z. Wang, Trastuzumab mechanism of action; 20 years of research to unravel a dilemma, Cancers 13 (2021) 3540, https://doi.org/10.3390/cancers13143540.
[12] O. Vaillant, K.E. Cheikh, D. Warther, D. Brevet, M. Maynadier, E. Bouffard, et al., Mannose-6-phosphate receptor: a target for theranostics of prostate cancer, Angew. Chem. Int. Ed. 54 (2015) 5952–5956, https://doi.org/10.1002/anie.201500286.
[13] A. Godefroy, M. Daurat, A. Da Silva, I. Basile, K. El Cheikh, C. Caillaud, et al., Mannose 6-phosphonate labelling: a key for processing the therapeutic enzyme in Pompe disease, J. Cell. Mol. Med. 23 (2019) 6499–6503, https://doi.org/10.1111/jcmm.14516.
[14] M. Daurat, C. Nguyen, S.D. Gil, V. Sol, V. Chaleix, C. Charnay, et al., The mannose 6-phosphate receptor targeted with porphyrin-based periodic mesoporous organosilica nanoparticles for rhabdomyosarcoma theranostics, Biomater. Sci. 8 (2020) 3678–3684, https://doi.org/10.1039/D0BM00586J.
[15] I. Basile, A. Da Silva, K. El Cheikh, A. Godefroy, M. Daurat, A. Harmois, et al., Efficient therapy for refractory Pompe disease by mannose 6-phosphate analogue grafting on. acid α-glucosidase, J. Control. Release 269 (2018) 15–23, https://doi.org/10.1016/j.jconrel.2017.10.043.
[16] E. Bouffard, C. Mauriello Jimenez, K. El Cheikh, M. Maynadier, I. Basile, L. Raehm, et al., Efficient photodynamic therapy of prostate cancer cells through an improved targeting of the cation-independent mannose 6-phosphate receptor, Int. J. Mol. Sci. 20 (2019) 2809, https://doi.org/10.3390/ijms20112809.

[17] A. Jeanjean, M. Gary-Bobo, P. Nirdé, S. Leiris, M. Garcia, A. Morère, Synthesis of new sulfonate and phosphonate derivatives for cation-independent mannose 6-phosphate receptor targeting, Bioorg. Med. Chem. Lett. 18 (2008) 6240–6243, https://doi.org/10.1016/j.bmcl.2008.09.101.

[18] A.K. Macioła, M.A. Pietrzak, P. Kosson, M. Czarnocki-Cieciura, K. Śmietanka, Z. Minta, et al., The length of N-glycans of recombinant H5N1 hemagglutinin influences the oligomerization and immunogenicity of vaccine antigen, Front. Immunol. 8 (2017) 444, https://doi.org/10.3389/fimmu.2017.00444.

[19] B. Ramadas, P. Kumar Pain, D. Manna, LYTACs: an emerging tool for the degradation of non-cytosolic proteins, ChemMedChem 16 (2021) 2951–2953, https://doi.org/10.1002/cmdc.202100393.

[20] A.L. Hopkins, C.R. Groom, The druggable genome, Nat. Rev. Drug Discov. 1 (2002) 727–730, https://doi.org/10.1038/nrd892.

[21] K.J. Brown, H. Seol, D.K. Pillai, B.-J. Sankoorikal, C.A. Formolo, J. Mac, et al., The human secretome atlas initiative: implications in health and disease conditions, Biochim. Biophys. Acta BBA - Proteins Proteom. 1834 (2013) 2454–2461, https://doi.org/10.1016/j.bbapap.2013.04.007.